



Published in final edited form as:

*Mol Psychiatry*. 2021 August ; 26(8): 4417–4430. doi:10.1038/s41380-019-0620-0.

## A network of phosphatidylinositol (4,5)-bisphosphate (PIP<sub>2</sub>) binding sites on the dopamine transporter regulates amphetamine behavior in *Drosophila Melanogaster*

Andrea N. Belovich<sup>#1</sup>, Jenny I. Aguilar<sup>#2,3</sup>, Samuel J. Mabry<sup>3</sup>, Mary H. Cheng<sup>4</sup>, Daniele Zanella<sup>3</sup>, Peter J. Hamilton<sup>5</sup>, Daniel J. Stanislawski<sup>6</sup>, Aparna Shekar<sup>2,3</sup>, James D. Foster<sup>6</sup>, Ivet Bahar<sup>4</sup>, Heinrich J. G. Matthies<sup>3</sup>, Aurelio Galli<sup>3</sup>

<sup>1</sup>Department of Pharmacology, Idaho College of Osteopathic Medicine, Meridian, ID, USA

<sup>2</sup>Department of Pharmacology, Vanderbilt University, Nashville, TN, USA

<sup>3</sup>Department of Surgery, University of Alabama at Birmingham, Birmingham, AL, USA

<sup>4</sup>Department of Computational and Systems Biology, School of Medicine, University of Pittsburgh, Pittsburgh, PA, USA

<sup>5</sup>Department of Anatomy and Neurobiology, Virginia Commonwealth University School of Medicine, Richmond, VA, USA

<sup>6</sup>Department of Biomedical Sciences, University of North Dakota School of Medicine and Health Sciences, Grand Forks, ND, USA

# These authors contributed equally to this work.

### Abstract

Reward modulates the saliency of a specific drug exposure and is essential for the transition to addiction. Numerous human PET–fMRI studies establish a link between midbrain dopamine (DA) release, DA transporter (DAT) availability, and reward responses. However, how and whether DAT function and regulation directly participate in reward processes remains elusive. Here, we developed a novel experimental paradigm in *Drosophila melanogaster* to study the mechanisms underlying the psychomotor and rewarding properties of amphetamine (AMPH). AMPH principally mediates its pharmacological and behavioral effects by increasing DA availability through the reversal of DAT function (DA efflux). We have previously shown that the phospholipid, phosphatidylinositol (4, 5)-bisphosphate (PIP<sub>2</sub>), directly interacts with the DAT

---

Jenny I. Aguilar [jenny.i.aguilar@vanderbilt.edu](mailto:jenny.i.aguilar@vanderbilt.edu).

These authors jointly supervised this work: Heinrich J. G. Matthies, Aurelio Galli

**Author contributions** JIA, AG, and HJGM conceptualized the study. JIA, ANB, SJM, MHC, DZ, PJH, DJS, AS, and HJGM carried out the experiments. JIA and AG conducted formal analyses of the data. JIA, AG, and HJGM provided conceptual advice and edited the manuscript. JIA and AG prepared data and figures and wrote the manuscript. AG and HJGM acquired funding and supervised the study. All authors contributed to the editing and review of the manuscript.

Compliance with ethical standards

**Publisher's note** Springer Nature remains neutral with regard to jurisdictional claims in published maps and institutional affiliations.

**Supplementary information** The online version of this article (<https://doi.org/10.1038/s41380-019-0620-0>) contains supplementary material, which is available to authorized users.

**Conflict of interest** The authors declare that they have no conflict of interest.

N-terminus to support DA efflux in response to AMPH. In this study, we demonstrate that the interaction of PIP<sub>2</sub> with the DAT N-terminus is critical for AMPH-induced DAT phosphorylation, a process required for DA efflux. We showed that PIP<sub>2</sub> also interacts with intracellular loop 4 at R443. Further, we identified that R443 electrostatically regulates DA efflux as part of a coordinated interaction with the phosphorylated N-terminus. In *Drosophila*, we determined that a neutralizing substitution at R443 inhibited the psychomotor actions of AMPH. We associated this inhibition with a decrease in AMPH-induced DA efflux in isolated fly brains. Notably, we showed that the electrostatic interactions of R443 specifically regulate the rewarding properties of AMPH without affecting AMPH aversion. We present the first evidence linking PIP<sub>2</sub>, DAT, DA efflux, and phosphorylation processes with AMPH reward.

---

## Introduction

Overshadowed by the current opioid epidemic, the resurgence of amphetamine (AMPH) and its derivatives (e.g., methamphetamine) in the United States has gone largely underreported [1]. While AMPHs are used clinically, the potential for AMPH abuse and dependency is high [2]. Underscoring this possibility is the observation that there are 37 million illicit AMPH users globally [3].

AMPH's rewarding and reinforcing effects, as well as its psychomotor stimulant properties, are associated with its ability to increase extracellular dopamine (DA) levels [4, 5]. AMPH perturbs DA homeostasis maintained by the DA transporter (DAT) as a competitive inhibitor and substrate of the DAT. The DAT is a presynaptic membrane protein that, under normal physiological conditions, drives the high-affinity transport (reuptake) of synaptically released DA, thereby regulating the spatial and temporal dynamics of extracellular DA levels. AMPH alters psychomotor behaviors, at least in part, by promoting the reversal of the DAT function (a nonvesicular event), here defined as DA efflux. Indeed, selective inhibition of DA efflux impairs AMPH psychomotor behaviors [6, 7]. Thus, in order to develop pharmacotherapies that mechanistically target and limit AMPH action (i.e., DA efflux), it is critical to understand how AMPH alters DAT function.

DA efflux is regulated by several molecular mechanisms and protein posttranslational modifications. We and others have shown that phosphorylation of the DAT N-terminus is required for AMPH-induced DA efflux [8, 9]. This phosphorylation process is mediated by several kinases, protein-protein interactions, as well as protein-lipid interactions [10–16]. Various other proteins and lipids regulate DA efflux through DAT association, including syntaxin 1 (SYN1) [12, 13, 17], G protein  $\beta\gamma$  subunits (G $\beta\gamma$ ) [14, 18], and phosphatidylinositol (4,5)-biphosphate (PIP<sub>2</sub>) [6].

Phospholipid molecules are an integral component of cell function and metabolism [19, 20], comprising ~50% of the plasma membrane. Among these, PIP<sub>2</sub> is the principal substrate of receptor-stimulated phospholipases C and the precursor to second messengers inositol trisphosphate (IP<sub>3</sub>), diacylglycerol, and phosphatidylinositol (3,4,5)-trisphosphate (PIP<sub>3</sub>). Moreover, PIP<sub>2</sub> itself acts as a second messenger and cofactor, regulating protein function [19, 21–24] and trafficking [25]. In addition, PIP<sub>2</sub>, through its electrostatic interactions, has been shown to modulate the function of ion channels and transporters, including the

serotonin transporter [19, 26] and the DAT [6]. In earlier studies, we have shown that PIP<sub>2</sub> directly interacts with the DAT through electrostatic interactions with basic, positively charged DAT N-terminal residues (Lys3 and Lys5). Substitution of these residues with uncharged amino acids decreases DAT/PIP<sub>2</sub> interactions, and AMPH-induced DA efflux and behaviors [6]. This was the first demonstration that PIP<sub>2</sub>, through its interaction with a plasma membrane protein, regulates DA-associated behaviors, underscoring the importance of elucidating the mechanism through which PIP<sub>2</sub> regulates DAT function and DAT-associated behaviors.

Recently, in silico experiments pointed to the possibility that PIP<sub>2</sub> also associates with the DAT intracellular loop 4 (IL4; specifically at R443) to regulate conformational rearrangements of the DAT N-terminus [27]. These simulations proposed that the interaction between the N-terminus and IL4, mediated by PIP<sub>2</sub>, may coordinate the dynamics of the intracellular gate. However, the biochemical, physiological, or behavioral relevance of these findings remained unclear. Using a combination of in silico and biochemical assays, we show that R443 physically interacts with PIP<sub>2</sub> as well as the N-terminus. We demonstrate in silico, in vitro, and ex vivo that R443 electrostatic interactions with PIP<sub>2</sub> and the N-terminus are required for specific DAT conformations that support DAT-mediated DA efflux in response to AMPH. In *Drosophila*, these interactions regulate fundamental behaviors, such as AMPH-induced hyperlocomotion and, notably, the rewarding properties of AMPH. Disrupting R443 electrostatic interactions does not affect the physiological function of the DAT, namely, uptake, nor basal locomotion. Thus, we have uncovered how a single residue in DAT IL4, R443 modulates AMPH actions, including reward.

## Materials and methods

### Cell culture

pCIHygro expression vector was engineered to contain synhDAT WT (hDAT WT), synhDAT S/D (Ser 2, 4, 7, 12, 13 mutated to Asp; hDAT S/D), synhDAT R443A (Arg443 mutated to Ala; hDAT R443A), and synhDAT S/D R443A (hDAT S/D R443A). Vector DNA was transfected into Chinese hamster ovary cells as previously described [28].

### <sup>3</sup>H[DA] uptake assays

Cells were washed and equilibrated in KRH (37 °C, 5 min) buffer composed of (in mM): 130 NaCl, 25 HEPES, 4.8 KCl, 1.2 KH<sub>2</sub>PO<sub>4</sub>, 1.1 MgSO<sub>4</sub>, 2.2 CaCl<sub>2</sub>, 10 d-glucose, 0.1 ascorbic acid, 0.1 pargyline, and 1.0 tropolone (pH 7.4). DA uptake kinetics were performed from 10 nM to 10 μM [<sup>3</sup>H] DA (PerkinElmer Life Sciences, Waltham, MA) as previously described [6].

### Amperometry and patch-clamp electrophysiology

Cells were washed with 37 °C Lub's external solution composed of (in mM): 130 NaCl, 1.5 CaCl<sub>2</sub>, 0.5 MgSO<sub>4</sub>, 1.3 KH<sub>2</sub>PO<sub>4</sub>, 10 HEPES, and 34 d-glucose (pH 7.4; 300–310 mOsm/L). Quartz patch pipettes were used to intracellularly load DA (2 mM, Sigma-Aldrich, St. Louis, MO) and/or PIP<sub>2</sub> inhibitory/control peptides (3 μM pal-HRQKHF<sub>2</sub>KRR or pal-HAQKHFEAAA) in internal solution containing (in mM): 110 KCl, 10 NaCl, 2

MgCl<sub>2</sub>, 0.1 CaCl<sub>2</sub>, 1.1 EGTA, 10 HEPES, 30 d-glucose, and 2.0 DA (pH 7.4; 280–290 mOsm/L). To record AMPH-induced DA efflux (10 μM), a carbon fiber electrode held at +600 mV was juxtaposed to cells as previously described [6].

### Biotinylation assays

Cells were washed with 4 °C phosphate-buffered saline supplemented with 0.9 mM CaCl<sub>2</sub> and 0.49 mM MgCl<sub>2</sub>, incubated in 1.0 mg/ml sulfosuccinimidyl-2-(biotinamido)ethyl-1,3-dithiopropionate-biotin (sulfo-NHS-SS-biotin; Pierce, Rockford, IL) and processed as previously described [28]. Membranes were immunoblotted for DAT (1:1000) (MAB369; Millipore, Billerica, MA) and β-actin (1:5000) (A5441; Sigma-Aldrich; St. Louis, MO), and then quantified as previously described [28].

### Immunoprecipitation assay

Cells expressing 6X-His, eGFP-tagged hDAT variants were lysed in buffer containing (mM): 20 Tris, 100 NaCl, and 20 n-dodecyl-β-D-maltopyranoside supplemented with 10% glycerol and protease inhibitor cocktail (1:100; Sigma-Aldrich, St. Louis, MO). Equivalent hDAT concentrations were isolated using batch cobalt-based immobilized metal affinity chromatography. Cobalt beads were washed, incubated for 4 h with 1 μM BODIPY<sup>®</sup> TMR Phosphatidylinositol 4,5-bisphosphate, washed, and eluted in buffer supplemented with 300 mM Imidazole. Eluates were assayed in a TECAN Infinite 200 Pro microplate reader for eGFP (ex 454/em 505 ± 9 nm) and PIP<sub>2</sub> (ex 542/em 574 ± 9 nm).

### DAT phosphorylation

hDAT WT, hDAT K/A, and hDAT K/N cDNAs were generated within pcDNA 3.0 plasmid using site-directed mutagenesis. Griptite 293 MSR cells (Thermo Fisher Scientific, Grand Island, NY) were transfected and metabolically labeled with <sup>32</sup>PO<sub>4</sub> (>8500 Ci/mmol, PerkinElmer) as described previously [9]. DATs were immunoprecipitated with DAT C-terminal antibody C-20 (1433, Santa Cruz Biotech; Santa Cruz, CA) crosslinked to protein A sepharose followed by SDS-PAGE and autoradiography.

### *Drosophila melanogaster* rearing and stocks

All *Drosophila melanogaster* strains were grown and maintained on standard cornmeal-molasses media at 25 °C under a 12:12 h light-dark schedule. Fly stocks include

*w*<sup>1118</sup> (Bloomington Indiana Stock Center (BI) 6326), TH-GAL4 (BI 8848), DAT<sup>MB07315</sup> (BI 25547), UAS-mCherry (Kyoto Stock Center 109594), M[vas-int.Dm]ZH-2A; M [3xP3-RFP.attP]ZH-22A (BI 24481) and *DAT*<sup>f<sup>inn</sup></sup> (dDAT KO). *Drosophila* expressing homozygous dDAT null allele *DAT*<sup>f<sup>inn</sup></sup> (dDAT KO) [29], TH-Gal4 [30], and UAS-mCherry were outcrossed to control lines for ten generations. Transgenes were cloned into pBI-UASC [31] and constructs were injected into embryos from BI 24481 (Rainbow Transgenic Flies Inc; Camarillo, CA). Flies containing transgenes were outcrossed to dDAT KO flies (in *w*<sup>1118</sup> background) for ten generations. Final transgene generations were crossed to dDAT KO/TH-GAL4 flies.

### **<sup>3</sup>H[DA] *Drosophila* uptake assays**

*Drosophila* male brains were dissected quickly in ice-cold Schneider's *Drosophila* Medium (Thermo Fisher Scientific) supplemented with 1.5% BSA. Single point DA uptake was measured by preincubating brains in either vehicle or 100  $\mu$ M cocaine for 10 min followed by 200 nM [<sup>3</sup>H]DA, as previously described [28]. Cocaine values were subtracted from vehicle values to determine specific counts.

### ***Drosophila* amperometry assays**

*Drosophila* male brains were dissected in ice-cold Schneider's *Drosophila* Medium supplemented with 1.5% BSA. Whole brains were placed in a mesh holder in Lub's external solution (see previous). A carbon fiber electrode held at +600 mV was positioned in the TH-positive PPL1 DA neuronal region and DA efflux was recorded as previously described [28].

### ***Drosophila* locomotion analysis**

*Drosophila* male flies were transferred individually to activity tubes containing standard food. TriKinetics *Drosophila* Activity Monitoring system (Waltham, MA) was used to measure basal and AMPH-induced locomotion, as previously described [17, 32].

### ***Drosophila* two-choice AMPH administration paradigm**

To measure AMPH preference in *Drosophila*, we built custom vials to measure liquid food consumption from volumetric capillaries. Each vial contained two volumetric capillaries: capillary A (100 mM sucrose) and capillary B (100 mM sucrose; 500  $\mu$ M blue dye). Food consumption was measured every 24 h when capillaries were replaced and refilled. Adult male flies were individually transferred to vials and acclimated to liquid food for 24 h. Baseline preference for capillary A and capillary B was assayed at 48 h. To determine AMPH preference, in experimental groups, capillary B was supplemented with AMPH (1 or 10 mM) and measured at 72 h. In control groups, capillary B was supplemented with vehicle (water) and measured at 72 h. Preference was determined as consumption of capillary B over total consumption (capillary A and capillary B) at 48 h (baseline) versus 72 h (preference).

### **Molecular dynamics (MD) simulations**

The full length hDAT was taken from previous study [33]. Four simulation systems were constructed: hDAT WT, hDAT R443A, hDAT S/D (Ser 2, 4, 7, 12, and 13 mutated to Asp), and hDAT S/D R443A. Transporters were embedded into neuronal membrane/lipids composed of 1-palmitoyl-2-oleoyl-sn-glycero-3-phosphoethanolamine and -phosphocholine, cholesterol, palmitoyl-oleoyl-phosphatidylinositol, and phosphatidylinositol 4,5-bisphosphate (PIP<sub>2</sub>) using CHARMM-GUI Membrane Builder module [34]. The lipid composition accounted for the asymmetric lipid distribution of neuronal membranes, as done previously [35]. Fully equilibrated TIP3P waters were added to build a simulation box of  $\sim 102 \times 102 \times 140$  Å, Na<sup>+</sup> and Cl<sup>-</sup> ions were added to obtain a 0.15 M neutral solution. Each simulation system contained  $\sim 134,000$  atoms,  $\sim 290$  lipid molecules, and 30,000 water molecules. All simulations were performed using the MD NAMD package [36] as previously [35]. For each system, two or three

independent runs of up to 200 ns were performed. The probability of PIP<sub>2</sub> binding was evaluated as the frequency of PIP<sub>2</sub>/DAT contacts; mainly, the fraction of 0.2 ns snapshots where PIP<sub>2</sub> was located within 4.0 Å from any DAT atom.

### N-terminus/IL4 binding assay

The hDAT WT or hDAT S/D (Ser 2, 4, 7, 12, and 13 mutated to Asp) N-terminus were cloned into pAT109 with a N-terminus GST and C-terminus His-tag. Proteins were expressed in B121(DE3) *E. coli*. Bacteria were induced with 0.5 mM isopropylβ-d-thiogalactopyranoside, pelleted, and lysed with lysozyme and 1% Triton-X100. Supernatants were isolated and bound to HisPur Cobalt Resin (Thermo Fisher Scientific), eluted with 0.5 M imidazole, dialyzed and applied to a glutathione column (GE Health-care Life Sciences, Chicago, IL). Protein was eluted with 10 mM glutathione, dialyzed, centrifuged, and protein quantified. Soluble, fluorescent IL4 (rhodamine-(PEG×3)-IDFQLLHRHRE) was synthesized by the peptide synthesis core at the University of Texas Southwestern. N-terminus of hDAT (WT and S/D) (2 μM) and IL4 (3 μM) were incubated for 2 h at RT in 25 mM HEPES (pH 7.2), 2 mM DTT, and 15 mM NaCl. Magnetic cobalt loaded beads were applied, incubated for 30 min, and washed three times in binding buffer. Beads were eluted with 0.3 M imidazole and assayed for fluorescence using TECAN Infinite 200 Pro microplate (ex 546/em 579 ± 9 nm).

### Statistical methods

Both animal and cell studies were designed using statistical power calculations considering means and standard errors from preliminary data. For example, our calculation rendered a minimum sample size of  $n = 6$  for ex vivo animal studies (power = 80%,  $\alpha = 0.05$ ). We estimated a maximum attrition of 33%; thus, we needed ten animals per group. Shapiro–Wilk normality tests were performed to evaluate sample distributions. Appropriate nonparametric tests were performed to compare samples with unequal variances. Otherwise parametric tests were used to compare data. Experiments were performed at random, except when indicated. In such cases, experiments were performed paired. Appropriate statistical analyses were conducted to reflect the paradigm used. Preference assays were performed blinded to genotype. All other animal studies were performed unblinded.

## Results

### N-terminus/PIP<sub>2</sub> interactions are required for AMPH-induced DAT phosphorylation

We have previously shown that neutralizing substitutions of Lys3 and Lys5 disrupt N-terminus/PIP<sub>2</sub> interactions and DA efflux [6]. Here, we sought to understand the molecular mechanism through which N-terminus/PIP<sub>2</sub> interactions regulate DA efflux. Specifically, does the interaction between the N-terminus DAT and PIP<sub>2</sub> support DAT phosphorylation, which is pivotal for robust AMPH-induced DA efflux [8]? To address this question, we disrupted N-terminus/PIP<sub>2</sub> interactions using hDAT K/A and hDAT K/N cells, where Lys3 and Lys5 were substituted for Ala or Asn, respectively, and measured DAT phosphorylation in response to AMPH (10 μM, 30 min) relative to hDAT WT cells. We quantified DAT phosphorylation by metabolic labeling (<sup>32</sup>PO<sub>4</sub>) as illustrated in representative autoradiographs under vehicle and AMPH conditions (Fig. 1a, top left).

The corresponding hDAT immunoblots for these autoradiographs are shown below (Fig. 1a, bottom left). Post AMPH treatment, hDAT WT cells displayed an increase in hDAT phosphorylation relative to vehicle-treated hDAT WT cells ( $p = 0.002$ ). In contrast, neither hDAT K/A nor hDAT K/N cells displayed a significant increase in hDAT phosphorylation in response to AMPH ( $p > 0.05$ ). Vehicle-treated (baseline) hDAT phosphorylation was comparable for hDAT WT, hDAT K/A and hDAT K/N ( $p > 0.05$ ) (Fig. 1a, right). Since Lys3 and Lys5 on the N-terminus are required for PIP<sub>2</sub> binding, these data suggest that the interaction between the N-terminus and PIP<sub>2</sub> is required for AMPH to elicit DAT phosphorylation.

Given PIP<sub>2</sub>'s integral role in DAT phosphorylation, we next sought to understand whether DAT/PIP<sub>2</sub> interactions were required for the reverse transport of DA by phosphorylated DAT. We used amperometry to measure DA efflux in response to AMPH (10  $\mu$ M) in hDAT WT cells and in cells where all N-terminal serines [2, 4, 7, 12, 13] were mutated to Asp (hDAT S/D) to mimic N-terminus phosphorylation. We depleted PIP<sub>2</sub>, thereby disrupting DAT/PIP<sub>2</sub> interactions with phenylarsine oxide (PAO, 20  $\mu$ M, 10 min), a PI-4 kinase inhibitor, which limits the synthesis of PIP<sub>2</sub> from phosphatidylinositol and effectively decreases PIP<sub>2</sub> levels. Consistent with our previous findings in hDAT WT cells [6], PIP<sub>2</sub> depletion by PAO pretreatment significantly reduced AMPH-induced DA efflux compared with vehicle conditions (Fig. 1b, top) ( $p = 0.04$ ). In contrast, in hDAT S/D cells PAO did not significantly reduce AMPH-induced DA efflux compared with vehicle (Fig. 1b, bottom) ( $p > 0.05$ ). Thus, our data strongly suggest that once DAT N-terminus phosphorylation occurs, DAT/PIP<sub>2</sub> interactions do not regulate DA efflux (Fig. 1b, right).

To validate these findings further, we sequestered PIP<sub>2</sub> at the plasma membrane with a basic peptide (pal-HRQKHFEEKRR), which consists of a palmitic acid, a fatty acid moiety that tethers the peptide to the plasma membrane and the putative PIP<sub>2</sub> binding domain of the Kv7.2 channel [37]. This pal-HRQKHFEEKRR acts as a competitive inhibitor, sequestering plasma membrane PIP<sub>2</sub>, and subsequently reducing AMPH-induced DA efflux in hDAT WT cells [6]. Here, we perfused hDAT S/D cells with DA and either the basic peptide pal-HRQKHFEEKRR (3  $\mu$ M, 10 min) or the control peptide pal-HAQKHFEEAAA (3  $\mu$ M, 10 min) using a whole-cell electrode while recording DA efflux with an amperometric electrode (Fig. 1c, left). We found that pal-HRQKHFEEKRR did not significantly change DA efflux relative to control peptide (Fig. 1c, right). Together, these data underscore that PIP<sub>2</sub> interactions are unlikely to regulate DA efflux once DAT is phosphorylated.

#### **R443 electrostatic interactions coordinate AMPH-induced DA efflux in vitro**

Increasing evidence from TRPV1, Kir<sub>2.1</sub> and other channels suggest that the effect of PIP<sub>2</sub> is mediated by multiple binding sites that may have different and/or interacting functions [38]. Thus, we sought to understand the contribution of other putative PIP<sub>2</sub> binding sites to reverse transport of DA. PIP<sub>2</sub> binds basic amino acids, frequently in the proximity of hydrophobic amino acids [19, 20]. The fourth intracellular loop (IL4) of the DAT contains a basic motif (H442-R443-H444-R445) surrounded by hydrophobic residues, thus, a likely site for PIP<sub>2</sub> binding. Indeed, our molecular dynamic simulations (see below), as well as others, predicted that the IL4 and more specifically, R443, is enriched and interacts with

PIP<sub>2</sub> lipids [27]. To test whether this possibility had biological and functional relevance, we measured the effect of a charge-neutralizing substitution of R443 to Ala (R443A) on DAT/PIP<sub>2</sub> interactions. Purified His-eGFP-tagged hDAT WT or hDAT R443A was incubated with a water-soluble analog of PIP<sub>2</sub> conjugated to an orange fluorophore (BODIPY<sup>®</sup> TMR-PIP<sub>2</sub>). Protein–lipid complexes were pelleted and PIP<sub>2</sub> binding was assayed as a ratio of PIP<sub>2</sub> to eGFP fluorescence. hDAT R443A displayed a significant  $34.8 \pm 9.9\%$  reduction in PIP<sub>2</sub> binding compared with hDAT WT ( $p = 0.007$ ) (Fig. 2a). The His-eGFP tag (negative control) had significantly diminished PIP<sub>2</sub> binding compared with hDAT WT, as well as to hDAT R443A. These data demonstrate that R443 contributes to the DAT/PIP<sub>2</sub> binding network.

In order to determine whether DAT functions are altered by disrupting this IL4/PIP<sub>2</sub> association, we first measured [<sup>3</sup>H]DA uptake in both hDAT WT and hDAT R443A cells. DA uptake kinetic curves for hDAT WT and hDAT R443A cells show that DA uptake is comparable through a range of concentrations ( $p > 0.05$ ) (Fig. 2b, top). In addition, neither the maximal velocity of DA uptake ( $V_{\max}$ ) nor apparent affinity for DA ( $K_m$ ) in hDAT R443A cells were significantly different from that of hDAT WT ( $p > 0.05$ ) (Fig. 2b, bottom). Thus, DA uptake is not regulated by the electrostatic interactions of R443.

Considering our previous findings that N-terminus/PIP<sub>2</sub> interactions support AMPH actions [6], we reasoned that disrupting IL4/PIP<sub>2</sub> interactions might alter the ability of AMPH to cause DA efflux. Figure 2c (left) displays representative amperometric traces recorded from hDAT WT and hDAT R443A upon AMPH application. hDAT R443A cells displayed a significant  $50.6 \pm 15.1\%$  decrease in AMPH-induced DA efflux relative to hDAT WT ( $p = 0.003$ ) (Fig. 2c, right). The disruption of the R443A mutation on DA efflux was so robust that PAO-mediated PIP<sub>2</sub> depletion in hDAT R443A cells (as described above) did not further reduce DA efflux compared with vehicle ( $p > 0.05$ ; Supplementary Fig. 1, bottom). In contrast, PAO significantly reduced AMPH-induced DA efflux in hDAT WT cells compared with vehicle ( $p = 0.04$ ; Supplementary Fig. 1, top). Thus, the electrostatic interactions of R443 with PIP<sub>2</sub> and/or other negatively charged motifs of the DAT regulate the reverse transport of DA (Supplementary Fig. 1, right).

Although we demonstrate no differences in DA uptake between hDAT WT and hDAT R443A, we used cell-surface biotinylation to confirm that this reduction in DA efflux was not due to changes in DAT plasma membrane expression. Surface fractions for hDAT WT and hDAT R443A were quantitated, normalized to total DAT (glycosylated), and expressed as a ratio of hDAT WT (Fig. 2d). This analysis yielded no significant differences in hDAT R443A and hDAT WT expression ( $p > 0.05$ ).

### **N-terminus phosphorylation and R443 electrostatic interactions are necessary for DA efflux**

Given the fundamental role of DAT phosphorylation in supporting DA efflux, we reasoned that disrupting R443 electrostatic interactions would be ineffective in regulating this process once the N-terminus DAT was phosphorylated. To test this, we mutated R443 to Ala in the hDAT S/D background (hDAT S/D R443A). We first assessed whether this mutation affected



DAT surface expression. This charge-neutralizing substitution at R443 did not affect DAT expression compared with controls (hDAT S/D) (Fig. 3a,  $p > 0.05$ ).

We also quantified the forward transport of DA supported by cells expressing hDAT S/D R443A relative to hDAT S/D cells (Fig. 3b, top). [<sup>3</sup>H]DA uptake kinetic curves showed comparable uptake in hDAT S/D R443A compared with hDAT S/D cells through a range of DA concentrations ( $p > 0.05$ ) (Fig. 3b, top). The  $V_{\max}$  and  $K_m$  in hDAT S/D R443A were not significantly different from that of hDAT S/D cells ( $p > 0.05$ ) (Fig. 3b, bottom). Finally, we measured the reverse transport capacity of hDAT S/D R443A cells compared with hDAT S/D in response to AMPH. Representative amperometric traces illustrated a significant  $63.9 \pm 0.3\%$  reduction in DA efflux in hDAT S/D R443A cells compared with hDAT S/D cells ( $p = 0.0004$ ) (Fig. 3c). hDAT S/D R443A cells displayed amperometric currents in response to AMPH, which were comparable in magnitude to previous recordings from hDAT R443A cells (compare Fig. 3c to Fig. 2c). These data emphasize the role of R443 in DA efflux, even when N-terminus phosphorylation has occurred.

To determine whether other putative PIP<sub>2</sub> binding sites on the DAT could further modulate the decrease in DA efflux promoted by R443 substitution, we reduced PIP<sub>2</sub> levels in hDAT S/D R443A cells by either pretreating cells with PAO or through patch delivery of a PIP<sub>2</sub> sequestering peptide (pal-HRQKHFEKRR) and measured DA efflux. As shown previously, PAO significantly reduced AMPH-induced DA efflux in hDAT WT cells compared with vehicle ( $p = 0.001$ ; Supplementary Fig. 2A). Notably, PAO did not further inhibit DA efflux in hDAT S/D R443A cells compared with vehicle ( $p > 0.05$ ; Supplementary Fig. 2A). Similarly, we found that pal-HRQKHFEKRR significantly reduced DA efflux relative to control peptide in hDAT WT cells ( $p = 0.02$ , Supplementary Fig. 2B), but did not significantly affect DA efflux in hDAT S/D R443A cells ( $p > 0.05$ , Supplementary Fig. 2B). Together, these data illustrate that once PIP<sub>2</sub> binding to R443 is impaired, N-terminus phosphorylation does not rescue impairments in DA efflux, and other DAT/PIP<sub>2</sub> interactions do not further regulate reverse transport of DA. These data also raise the possibility that an electrostatic interaction between the positively charged R443 and negatively charged, phosphorylated N-terminus may be important to DA efflux.

Our MD simulations showed that PIP<sub>2</sub> coordinates the interactions between the N-terminus and IL4 (Supplementary Fig. 3A). However, once the N-terminus is phosphorylated, it interacts directly with IL4 (R443) displacing PIP<sub>2</sub> (Supplementary Fig. 3B, Supplementary Movie 1). Notably, we showed in vitro that pseudophosphorylation of the N-terminus significantly increases its affinity for IL4 ( $p < 0.0001$ ; Supplementary Fig. 3C). As indicated by our in vitro experiments, our MD simulations confirmed that a neutralizing substitution at R443 impairs the interaction between PIP<sub>2</sub> and IL4 (Supplementary Fig. 4A, Supplementary Movie 2). Furthermore, R443A substitution in the presence of N-terminal phosphorylation weakens and eventually impairs the interaction between the anionically charged N-terminus and IL4 (Supplementary Fig. 4B, Supplementary Movie 3), an interaction we show is required for DA efflux.

## Disrupting the electrostatic interactions of R443 limits central and behavioral responses to AMPH

We utilized the genetic tractability of *Drosophila melanogaster* to study the ex vivo and in vivo consequences of a charge-neutralizing substitution at R443. *Drosophila* is a powerful model system to study DA signaling in vivo due to conserved mechanisms of DA neurotransmission, including synthesis, packaging, and transport [39]. We used phiC31-based integration to insert our UAS-driven transgene of interest (hDAT WT or hDAT R443A) in the fly genome of a *Drosophila* DAT (dDAT) null background (*DAT<sup>flm</sup>*), as previously described [32].

We first determined whether hDAT R443A expressing flies supported normal DAT functions. We found that isolated hDAT R443A brains have comparable DA uptake to hDAT WT brains ( $p > 0.05$ ) (Fig. 4a). Next, we measured the reverse transport capacity of DAT in hDAT WT or hDAT R443A isolated fly brains using amperometry. Upon the addition of AMPH, DA efflux was measured from posterior inferior-lateral protocerebrum 1 (PPL1) neurons (Fig. 4b, white box inset), a dense cluster DA neurons that innervate the mushroom-body modulating reward and punishment learning [40–42]. Consistent with our in vitro data, hDAT R443A displayed a significant reduction in DA efflux compared with hDAT WT brains ( $p = 0.004$ ).

Consequently, we focused on understanding the role of DA efflux in complex behaviors using hDAT R443A flies. We first studied an elemental behavior regulated by DA, locomotion. Based on our new findings that hDAT R443A supports normal DA uptake in *Drosophila* brains, we hypothesized that hDAT R443A flies would have normal circadian locomotor activity. Consistent with our hypothesis, circadian locomotor activity in hDAT R443A flies did not significantly differ from that of hDAT WT flies (Fig. 4c,  $p > 0.05$ ).

Previous studies have shown that commonly abused drugs affect behavioral phenotypes in flies, similar to those observed in rodents and humans [29, 43, 44]. To this end, we and others have shown that acute AMPH exposure increases locomotor activity in *Drosophila* [4, 6, 7, 45]. AMPH elicits these behaviors by increasing levels of extracellular DA, a process mediated (at least in part) by DA efflux [5, 46]. We reasoned that given deficits in DA efflux in hDAT R443A flies, AMPH-induced hyperactivity would also be diminished in these animals. Exposure to AMPH (1 mM, 30 min) significantly increased activity in hDAT WT flies compared with vehicle (Fig. 4d,  $p = 0.0005$ ), but not in hDAT R443A flies relative to vehicle ( $p > 0.05$ ). Thus, charge-neutralizing R443 blunts the acute psychomotor response to AMPH.

### R443 electrostatic interactions selectively regulate AMPH preference

Reward is a fundamental behavior regulated across phyla by DA neurotransmission [47, 48]; however, the role of DA efflux in this process is not well understood. Increasing evidence supports DAT's role in regulating reward [49, 50]. Thus, we took advantage of our fly model to determine the role of DAT-mediated DA efflux in reward processes. To quantify possible differences in AMPH preference in hDAT WT and hDAT R443A flies, we adapted the CAPillary FEeding assay [51–53] to measure AMPH consumption. In this redesigned

paradigm, adult male flies were acclimated to custom-built testing chambers containing two capillaries filled with either (a) sucrose or (b) sucrose-blue food (Fig. 5a). Following this acclimation period, on day 1, baseline consumption, defined as a ratio of sucrose-blue ( $nL_{\text{blue}}$ ) to total food consumed ( $nL_T$ ), was measured. Consumption levels of 0.5 indicate no preference across the two capillaries. Levels greater than 0.5 indicate preference, and levels lower than 0.5 indicate aversion. On day 2, experimental groups were given the choice of (a) sucrose or (b) sucrose-blue food supplemented with AMPH (1 mM or 10 mM; solid lines). Notably, hDAT WT flies displayed preference for AMPH (day 2:  $0.62 \pm 0.04$ ) compared with baseline (day 1:  $0.46 \pm 0.03$ ;  $p = 0.005$ ) (Fig. 5b). To ensure that the increase in AMPH consumption was not due to a developed preference for sucrose-blue food, control groups (dashed lines) were given the choice of (a) sucrose or (b) sucrose-blue food supplemented with vehicle on day 2. hDAT WT control groups (dashed black lines) did not develop a preference for sucrose-blue food (day 1:  $0.46 \pm 0.03$  versus day 2:  $0.46 \pm 0.03$ ;  $p > 0.05$ ). These data confirm that hDAT WT animals displayed a preference specifically for 1 mM AMPH. Interestingly, hDAT R443A flies did not show preference for AMPH relative to baseline (red solid line,  $p > 0.05$ ). hDAT R443A control groups also did not develop a preference for sucrose-blue food (red dashed line,  $p > 0.05$ ). To account for potential changes in feeding behavior, we compared total food consumption across genotypes (hDAT WT versus hDAT R443A) and groups (control: vehicle versus experimental: 1 mM AMPH). Total food consumption on day 2 was not statistically different in control groups (lined bars) compared with AMPH groups (solid bars) in either hDAT WT or hDAT R443A flies (Supplementary Fig. 5A;  $p > 0.05$ ). Moreover, total food consumption in hDAT WT ( $1.40 \pm 0.15$ ) compared with hDAT R443A flies ( $1.32 \pm 0.10$ ) exposed to 1 mM AMPH was also not statistically different ( $p > 0.05$ ). Thus, there were no measurable changes in feeding across groups or genotypes. These data show that a single amino acid substitution at position R443 decreases the rewarding properties of AMPH in flies without altering food reward or consumption.

In hDAT WT flies, higher concentrations of AMPH (10 mM) resulted in a significant  $39.2 \pm 1.9\%$  decline in AMPH consumption compared with baseline (day 2 versus day 1,  $p = 0.0004$ ) (Fig. 5c). hDAT R443A flies also displayed an aversion for AMPH, where consumption decreased by  $33.8 \pm 3.9\%$  on day 2 compared with day 1 ( $p = 0.03$ ). Neither control groups for both hDAT WT or hDAT R443A saw a change in sucrose-blue food consumption on day 2 relative to baseline ( $p > 0.05$ ). Given AMPH's well-known anorexigenic effects [54], we confirmed that aversion for AMPH was not skewed by significant changes in total food consumption on day 2 relative to day 1, neither in hDAT WT nor hDAT R443A flies (Supplementary Fig. 5b,  $p > 0.05$ ). Therefore, an Arg at position 443 is a hDAT residue that regulates AMPH reward, although it does not modulate AMPH's aversive properties.

## Discussion

Within the central nervous system, psychostimulant exposure modifies phospholipid profiles in a brain region-dependent manner [55–57]. Phospholipid levels increase in response to psychostimulants in the striatum and hippocampus, regions critical for drug reward and reinstatement, respectively [55, 58]. In contrast, phospholipid levels decrease in the

cerebellum [58]. Altered phospholipid levels and metabolism have also been reported in psychostimulant users [57, 59]. These findings support the notion that psychostimulant action is regulated by phospholipids and, possibly, by the interaction of phospholipids with plasma membrane proteins. In this study, we sought to understand how phospholipids, as well as their association with the DAT, regulate the psychomotor and rewarding actions of AMPH.

We have previously shown that pharmacologically limiting PIP<sub>2</sub> availability impairs AMPH's actions at DAT [6], as well as its ability to induce hyperlocomotion. However, how the interaction between PIP<sub>2</sub> and the DAT N-terminus supported AMPH behaviors remained unclear. Here, we found that limiting PIP<sub>2</sub> binding through neutralizing substitutions of Lys3 and Lys5 at the N-terminus limits AMPH-induced DAT phosphorylation, which is required for AMPH actions [8–10]. Significantly, neither “sequestering” PIP<sub>2</sub> with a positively charged palmitoylated peptide nor pharmacologically depleting PIP<sub>2</sub> by inhibiting PIP<sub>2</sub> synthesis affected DA efflux once the DAT N-terminus had been pseudophosphorylated. Therefore, the electrostatic interactions between N-terminus Lys and PIP<sub>2</sub> regulate DAT phosphorylation. Moreover, following DAT phosphorylation, PIP<sub>2</sub> levels, as well as its interactions, are not critical to DA efflux.

Molecular dynamic simulations and biochemical experiments show that residue R443 also contributes to PIP<sub>2</sub> interactions. A neutralizing substitution at R443 (hDAT R443A) significantly decreased DAT/PIP<sub>2</sub> interactions. Specifically, this substitution was sufficient to disrupt the electrostatic interactions between R443 (IL4) and PIP<sub>2</sub>, as well as downregulate those between PIP<sub>2</sub> and N-terminus. Unsurprisingly, hDAT R443A displayed limited AMPH-induced DA efflux, suggesting that R443 electrostatic interactions are important for the reverse transport of DA.

Probing further the contribution of R443 to AMPH action, we found that a neutralizing substitution at R443 to Ala in a pseudophosphorylated hDAT (hDAT S/D) background (hDAT S/D R443A) reduced DA efflux relative hDAT S/D controls. Our MD simulations show that once phosphorylated, the N-terminus disrupts the interaction between IL4 and PIP<sub>2</sub>. Also, we show in vitro that pseudophosphorylation of the N-terminus increases its affinity for IL4. Thus, a neutralizing substitution at R443 limits the physical interaction of an anionically charged N-terminus (phosphorylated) with the positively charged motif at IL4, an interaction we believe is required for DA efflux and behaviors.

It is important to note that reducing PIP<sub>2</sub> levels in hDAT S/D R443A cells did not further impair DA efflux. Once R443 electrostatics are neutralized with Ala substitution, PIP<sub>2</sub> levels lose their ability to regulate DA efflux. However, in this model, we cannot exclude the possibility that the amino acids surrounding R443, in the positively charged motif (His442-Arg443-His444-Arg445), also contribute to DA efflux. It is also important to consider the role of other DAT interacting proteins, including SYN1 and Gβγ. SYN1 interacts with the DAT N-terminus to support AMPH-induced DA efflux [12, 13, 60]. In addition, Gβγ interacts with the carboxy terminus of DAT, whereby activation of Gβγ promotes AMPH-induced DA efflux and behaviors [14, 18]. The actions of both Gβγ and SYN1 are thought

to be modulated by PIP<sub>2</sub> [14, 18, 61]. Future studies are necessary to determine how and if these protein–protein and protein–lipid interactions work in concert to promote DA efflux.

Notably, in this study, we show that a neutralizing substitution of R443 in the DAT reduces the ability of AMPH to elicit psychomotor behaviors without altering basal locomotion. Locomotion is a fundamental behavior that enables seeking for rewarding stimuli including sex, food, and drugs. AMPH induces increased locomotor activity in *Drosophila* as in mammals [4, 6, 7, 62, 63]. We found that hDAT R443A *Drosophila* were insensitive to locomotor actions of AMPH. These data are consistent with our ex vivo findings showing that DA efflux was significantly diminished in hDAT R443A compared with hDAT WT *Drosophila* brain. Intrigued by these results, we further explored whether R443, as well as DA efflux, played a role in the rewarding properties of AMPH.

Reward modulates the saliency of a specific drug exposure and is essential for the transition from drug exposure to addiction [64]. We developed a new behavioral paradigm to measure AMPH preference in *Drosophila*. We show that a single amino acid substitution that disrupts IL4 electrostatic interactions, reduces DA efflux and preference for AMPH without affecting aversion. Numerous human PET-fMRI studies have established a link between midbrain DA release/DAT availability and reward responses [49, 50]. Recent findings showed that clinical subgroups with the lowest DAT levels displayed the lowest functional anticipatory reward activation [49]. Based on these findings, it is not surprising that we found that animals with limited physiological responses to AMPH (i.e., DA efflux) displayed a lack of preference for AMPH. Finally, previous findings demonstrated inverted responses to higher concentrations of AMPH [54, 65]. Here, in flies, we show that high AMPH concentrations cause aversion. In contrast to AMPH preference, in our animal model, neutralizing the electrostatic interaction of R443 did not affect aversion. Thus, AMPH aversion in *Drosophila* is likely mediated by mechanisms that are independent of reverse transport of DA and/or are DAT independent [66]. One possibility is that at higher concentrations, the bitter taste of AMPH itself drives an aversive response. Alternatively, AMPH aversion may also be regulated by glutamatergic and serotonergic inputs [67, 68] that are modified by AMPH and fine-tuned DA neurons. Recent studies in *Drosophila* illustrate that preference for other stimulants such as cocaine is sex-specific, thus, further studies to determine this potential contribution for AMPH preference are necessary.

We sought to understand the molecular mechanism through which structural domains of the DAT regulate the psychomotor and rewarding properties of AMPH. We developed a novel behavioral paradigm in *Drosophila* to quantify AMPH's rewarding properties by measuring relative preference for AMPH and associate it with the ability of AMPH to cause DA efflux in brain. We uncovered how a specific residue in the DAT tightly regulates DA efflux and the rewarding properties of the psychostimulant AMPH.

## Supplementary Material

Refer to Web version on PubMed Central for supplementary material.

## Acknowledgements

The authors would like to acknowledge Saunders Consulting for the help in editing this manuscript. Research reported in this publication was supported by NIH R01-DA038058 (AG), NIH R01-DA035263 (AG and HJGM), NIH K99/R00-DA045795 (PJH), NIH F31-MH114316 (JIA), NIH P41-GM103712 (IB), and NIH P30-DA035778 (IB). The content is solely the responsibility of the authors and does not necessarily represent the official views of the National Institutes of Health.

## References

1. Winkelman TNA, Admon LK, Jennings L, Shippee ND, Richardson CR, Bart G. Evaluation of amphetamine-related hospitalizations and associated clinical outcomes and costs in the United States. *JAMA Netw Open*. 2018;1:e183758.
2. Berman S, O'Neill J, Fears S, Bartzokis G, London ED. Abuse of amphetamines and structural abnormalities in the brain. *Ann N Y Acad Sci*. 2008;1141:195–220. [PubMed: 18991959]
3. UN Office DaC. World Drug Report 2017. Vienna, Austria: United Nations Publication; 2017. Report no.: 978–92-1-148291-1.
4. Freyberg Z, Sonders MS, Aguilar JI, Hiranita T, Karam CS, Flores J, et al. Mechanisms of amphetamine action illuminated through optical monitoring of dopamine synaptic vesicles in *Drosophila* brain. *Nat Commun*. 2016;7:10652. [PubMed: 26879809]
5. Sulzer D, Sonders MS, Poulsen NW, Galli A. Mechanisms of neurotransmitter release by amphetamines: a review. *Prog Neurobiol*. 2005;75:406–33. [PubMed: 15955613]
6. Hamilton PJ, Belovich AN, Khelashvili G, Saunders C, Erreger K, Javitch JA, et al. PIP2 regulates psychostimulant behaviors through its interaction with a membrane protein. *Nat Chem Biol*. 2014;10:582–9. [PubMed: 24880859]
7. Pizzo AB, Karam CS, Zhang Y, Yano H, Freyberg RJ, Karam DS, et al. The membrane raft protein Flotillin-1 is essential in dopamine neurons for amphetamine-induced behavior in *Drosophila*. *Mol Psychiatry*. 2013;18:824–33. [PubMed: 22710269]
8. Khoshbouei H, Sen N, Guptaroy B, Johnson L, Lund D, Gnegy ME, et al. N-terminal phosphorylation of the dopamine transporter is required for amphetamine-induced efflux. *PLoS Biol*. 2004;2: E78.
9. Cervinski MA, Foster JD, Vaughan RA. Psychoactive substrates stimulate dopamine transporter phosphorylation and down regulation by cocaine sensitive and protein kinase C dependent mechanisms. *J Biol Chem*. 2005;280:40442–9. [PubMed: 16204245]
10. Fog JU, Khoshbouei H, Holy M, Owens WA, Vaegter CB, Sen N, et al. Calmodulin kinase II interacts with the dopamine transporter C terminus to regulate amphetamine-induced reverse transport. *Neuron*. 2006;51:417–29. [PubMed: 16908408]
11. Johnson LA, Guptaroy B, Lund D, Shamban S, Gnegy ME. Regulation of amphetamine-stimulated dopamine efflux by protein kinase C beta. *J Biol Chem*. 2005;280:10914–9. [PubMed: 15647254]
12. Binda F, Dipace C, Bowton E, Robertson SD, Lute BJ, Fog JU, et al. Syntaxin 1A interaction with the dopamine transporter promotes amphetamine-induced dopamine efflux. *Mol Pharm*. 2008;74:1101–8.
13. Cervinski MA, Foster JD, Vaughan RA. Syntaxin 1A regulates dopamine transporter activity, phosphorylation and surface expression. *Neuroscience*. 2010;170:408–16. [PubMed: 20643191]
14. Mauna JC, Harris SS, Pino JA, Edwards CM, DeChellis-Marks MR, Bassi CD, et al. G protein betagamma subunits play a critical role in the actions of amphetamine. *Transl Psychiatry*. 2019;9:81. [PubMed: 30745563]
15. Granas C, Ferrer J, Loland CJ, Javitch JA, Gether U. N-terminal truncation of the dopamine transporter abolishes phorbol ester- and substance P receptor-stimulated phosphorylation without impairing transporter internalization. *J Biol Chem*. 2003;278: 4990–5000. [PubMed: 12464618]
16. Foster JD, Pananusorn B, Vaughan RA. Dopamine transporters are phosphorylated on N-terminal serines in rat striatum. *J Biol Chem*. 2002;277:25178–86. [PubMed: 11994276]
17. Cartier E, Hamilton PJ, Belovich AN, Shekar A, Campbell NG, Saunders C, et al. Rare autism-associated variants implicate syntaxin 1 (STX1 R26Q) phosphorylation and the dopamine

transporter (hDAT R51W) in dopamine neurotransmission and behaviors. *EBioMedicine*. 2015;2:135–46. [PubMed: 25774383]

18. Garcia-Olivares J, Baust T, Harris S, Hamilton P, Galli A, Amara SG, et al. Gbetagamma subunit activation promotes dopamine efflux through the dopamine transporter. *Mol Psychiatry*. 2017;22:1673–9. [PubMed: 28894302]
19. Suh BC, Hille B. PIP2 is a necessary cofactor for ion channel function: how and why? *Annu Rev Biophys*. 2008;37:175–95. [PubMed: 18573078]
20. McLaughlin S, Murray D. Plasma membrane phosphoinositide organization by protein electrostatics. *Nature*. 2005;438:605–11. [PubMed: 16319880]
21. Kadamur G, Ross EM. Mammalian phospholipase C. *Annu Rev Physiol*. 2013;75:127–54. [PubMed: 23140367]
22. Czech MP. PIP2 and PIP3: complex roles at the cell surface. *Cell*. 2000;100:603–6. [PubMed: 10761925]
23. Ben-Aissa K, Patino-Lopez G, Belkina NV, Maniti O, Rosales T, Hao JJ, et al. Activation of moesin, a protein that links actin cytoskeleton to the plasma membrane, occurs by phosphatidylinositol 4,5-bisphosphate (PIP2) binding sequentially to two sites and releasing an autoinhibitory linker. *J Biol Chem*. 2012;287:16311–23. [PubMed: 22433855]
24. Whorton MR, MacKinnon R. Crystal structure of the mammalian GIRK2 K<sup>+</sup> channel and gating regulation by G proteins, PIP2, and sodium. *Cell*. 2011;147:199–208. [PubMed: 21962516]
25. Thapa N, Anderson RA. PIP2 signaling, an integrator of cell polarity and vesicle trafficking in directionally migrating cells. *Cell Adh Migr*. 2012;6:409–12. [PubMed: 23076053]
26. Buchmayer F, Schicker K, Steinkellner T, Geier P, Stubiger G, Hamilton PJ, et al. Amphetamine actions at the serotonin transporter rely on the availability of phosphatidylinositol-4,5-bisphosphate. *PNAS*. 2013;110:11642–7. [PubMed: 23798435]
27. Khelashvili G, Stanley N, Sahai MA, Medina J, LeVine MV, Shi L, et al. Spontaneous inward opening of the dopamine transporter is triggered by PIP2-regulated dynamics of the N-terminus. *ACS Chem Neurosci*. 2015;6:1825–37. [PubMed: 26255829]
28. Campbell NG, Shekar A, Aguilar JJ, Peng D, Navratna V, Yang D, et al. Structural, functional, and behavioral insights of dopamine dysfunction revealed by a deletion in SLC6A3. *PNAS*. 2019;116:3853–62. [PubMed: 30755521]
29. Kume K, Kume S, Park SK, Hirsh J, Jackson FR. Dopamine is a regulator of arousal in the fruit fly. *J Neurosci*. 2005;25:7377–84. [PubMed: 16093388]
30. Friggi-Grelin F, Coulom H, Meller M, Gomez D, Hirsh J, Birman S. Targeted gene expression in *Drosophila* dopaminergic cells using regulatory sequences from tyrosine hydroxylase. *J Neurobiol*. 2003;54:618–27. [PubMed: 12555273]
31. Wang JW, Beck ES, McCabe BD. A modular toolset for recombination transgenesis and neurogenetic analysis of *Drosophila*. *PLoS One*. 2012;7:e42102.
32. Hamilton PJ, Campbell NG, Sharma S, Erreger K, Herborg Hansen F, Saunders C, et al. De novo mutation in the dopamine transporter gene associates dopamine dysfunction with autism spectrum disorder. *Mol Psychiatry*. 2013;18:1315–23. [PubMed: 23979605]
33. Cheng MH, Block E, Hu F, Cobanoglu MC, Sorkin A, Bahar I. Insights into the modulation of dopamine transporter function by amphetamine, orphenadrine, and cocaine binding. *Front Neurol*. 2015;6:134. [PubMed: 26106364]
34. Wu EL, Cheng X, Jo S, Rui H, Song KC, Dávila-Contreras EM, et al. CHARMM-GUI membrane builder toward realistic biological membrane simulations. *J Comput Chem*. 2014;35: 1997–2004. [PubMed: 25130509]
35. Cheng MH, Ponzoni L, Sorkina T, Lee JY, Zhang S, Sorkin A, et al. Trimerization of dopamine transporter triggered by AIM-100 binding: Molecular mechanism and effect of mutations. *Neuropharmacology*. 2019;107676.
36. Phillips JC, Braun R, Wang W, Gumbart J, Tajkhorshid E, Villa E, et al. Scalable molecular dynamics with NAMD. *J Comput Chem*. 2005;26:1781–802. [PubMed: 16222654]
37. Robbins J, Marsh SJ, Brown DA. Probing the regulation of M (Kv7) potassium channels in intact neurons with membrane-targeted peptides. *J Neurosci*. 2006;26:7950–61. [PubMed: 16870740]

38. Yu K, Jiang T, Cui Y, Tajkhorshid E, Hartzell HC. A network of phosphatidylinositol 4,5-bisphosphate binding sites regulate gating of the Ca<sup>2+</sup> activated Cl-channel ANO1 (TMEM16A). 2019; 625897. 10.1073/pnas.1904012116.
39. Yamamoto S, Seto ES. Dopamine dynamics and signaling in *Drosophila*: an overview of genes, drugs and behavioral paradigms. *Exp Anim*. 2014;63:107–19. [PubMed: 24770636]
40. Claridge-Chang A, Roorda RD, Vrontou E, Sjulson L, Li H, Hirsh J, et al. Writing memories with light-addressable reinforcement circuitry. *Cell*. 2009;139:405–15. [PubMed: 19837039]
41. Kirkhart C, Scott K. Gustatory learning and processing in the *Drosophila* mushroom bodies. *J Neurosci*. 2015;35:5950–8. [PubMed: 25878268]
42. Kaun KR, Azanchi R, Maung Z, Hirsh J, Heberlein U. A *Drosophila* model for alcohol reward. *Nat Neurosci*. 2011;14:612–9. [PubMed: 21499254]
43. Brand AH, Perrimon N. Targeted gene expression as a means of altering cell fates and generating dominant phenotypes. *Development*. 1993;118:401–15. [PubMed: 8223268]
44. McClung C, Hirsh J. Stereotypic behavioral responses to free-base cocaine and the development of behavioral sensitization in *Drosophila*. *Curr Biol*. 1998;8:109–12. [PubMed: 9427649]
45. Aguilar JI, Dunn M, Mingote S, Karam CS, Farino ZJ, Sonders MS, et al. Neuronal depolarization drives increased dopamine synaptic vesicle loading via VGLUT. *Neuron*. 2017;95: 1074–88 e7. [PubMed: 28823729]
46. Fleckenstein AE, Volz TJ, Riddle EL, Gibb JW, Hanson GR. New insights into the mechanism of action of amphetamines. *Annu Rev Pharm Toxicol*. 2007;47:681–98.
47. Arias-Carrion O, Stamelou M, Murillo-Rodriguez E, Menendez-Gonzalez M, Poppel E. Dopaminergic reward system: a short integrative review. *Int Arch Med*. 2010;3:24. [PubMed: 20925949]
48. Scaplen KM, Kaun KR. Reward from bugs to bipeds: a comparative approach to understanding how reward circuits function. *J Neurogenet*. 2016;30:133–48. [PubMed: 27328845]
49. Dubol M, Trichard C, Leroy C, Sandu AL, Rahim M, Granger B, et al. Dopamine transporter and reward anticipation in a dimensional perspective: a multimodal brain imaging study. *Neuropsychopharmacology*. 2018;43:820–7. [PubMed: 28829051]
50. Schott BH, Minuzzi L, Krebs RM, Elmenhorst D, Lang M, Winz OH, et al. Mesolimbic functional magnetic resonance imaging activations during reward anticipation correlate with reward-related ventral striatal dopamine release. *J Neurosci*. 2008;28:14311–9. [PubMed: 19109512]
51. Ja WW, Carvalho GB, Mak EM, de la Rosa NN, Fang AY, Liang JC, et al. Prandiology of *Drosophila* and the CAFE assay. *PNAS*. 2007;104:8253–6. [PubMed: 17494737]
52. Diegelmann S, Jansen A, Jois S, Kastenholz K, Velo Escarcena L, Strudthoff N, et al. The CApillary FEeder assay measures food intake in *Drosophila melanogaster*. *J Vis Exp*. 2017;121: 55024.
53. Devineni AV, Heberlein U. Preferential ethanol consumption in *Drosophila* models features of addiction. *Curr Biol*. 2009;19: 2126–32. [PubMed: 20005106]
54. Foltin RW. The behavioral pharmacology of anorexigenic drugs in nonhuman primates: 30 years of progress. *Behav Pharm*. 2012;23:461–77.
55. Cummings BS, Pati S, Sahin S, Scholpa NE, Monian P, Trinquero PM, et al. Differential effects of cocaine exposure on the abundance of phospholipid species in rat brain and blood. *Drug Alcohol Depend*. 2015;152:147–56. [PubMed: 25960140]
56. Ross BM, Turenne SD. Chronic cocaine administration reduces phospholipase A(2) activity in rat brain striatum. *Prostaglandins Leukot Ess Fat Acids*. 2002;66:479–83.
57. Leussen DC, Psychostimulants Rong. Brain membrane lipids and dopamine transmission. *J Biomolecular Res Therapeutics*. 2016;5:1000143.
58. Marchant NJ, Kaganovsky K, Shaham Y, Bossert JM. Role of corticostriatal circuits in context-induced reinstatement of drug seeking. *Brain Res*. 2015;1628:219–32. [PubMed: 25199590]
59. Ross BM, Moszczynska A, Peretti FJ, Adams V, Schmunk GA, Kalasinsky KS, et al. Decreased activity of brain phospholipid metabolic enzymes in human users of cocaine and methamphetamine. *Drug Alcohol Depend*. 2002;67:73–9. [PubMed: 12062780]



60. Lee KH, Kim MY, Kim DH, Lee YS. Syntaxin 1A and receptor for activated C kinase interact with the N-terminal region of human dopamine transporter. *Neurochem Res.* 2004;29:1405–9. [PubMed: 15202772]
61. Khelashvili G, Galli A, Weinstein H. Phosphatidylinositol 4,5-bisphosphate (PIP(2)) lipids regulate the phosphorylation of syntaxin N-terminus by modulating both its position and local structure. *Biochemistry.* 2012;51:7685–98. [PubMed: 22950482]
62. Amara SG, Kuhar MJ. Neurotransmitter transporters: recent progress. *Annu Rev Neurosci.* 1993;16:73–93. [PubMed: 8096377]
63. Giros B, Caron MG. Molecular characterization of the dopamine transporter. *Trends Pharm Sci.* 1993;14:43–9. [PubMed: 8480373]
64. Volkow ND, Fowler JS, Wang GJ. The addicted human brain viewed in the light of imaging studies: brain circuits and treatment strategies. *Neuropharmacology.* 2004;47 Suppl 1:3–13. [PubMed: 15464125]
65. Cabib S, Orsini C, Le Moal M, Piazza PV. Abolition and reversal of strain differences in behavioral responses to drugs of abuse after a brief experience. *Science.* 2000;289:463–5. [PubMed: 10903209]
66. O'Neill MF, Shaw G. Comparison of dopamine receptor antagonists on hyperlocomotion induced by cocaine, amphetamine, MK-801 and the dopamine D1 agonist C-APB in mice. *Psychopharmacology.* 1999;145:237–50.
67. Pignatelli M, Bonci A. Role of dopamine neurons in reward and aversion: a synaptic plasticity perspective. *Neuron.* 2015;86: 1145–57. [PubMed: 26050034]
68. Hu H. Reward and Aversion. *Annu Rev Neurosci.* 2016;39: 297–324. [PubMed: 27145915]

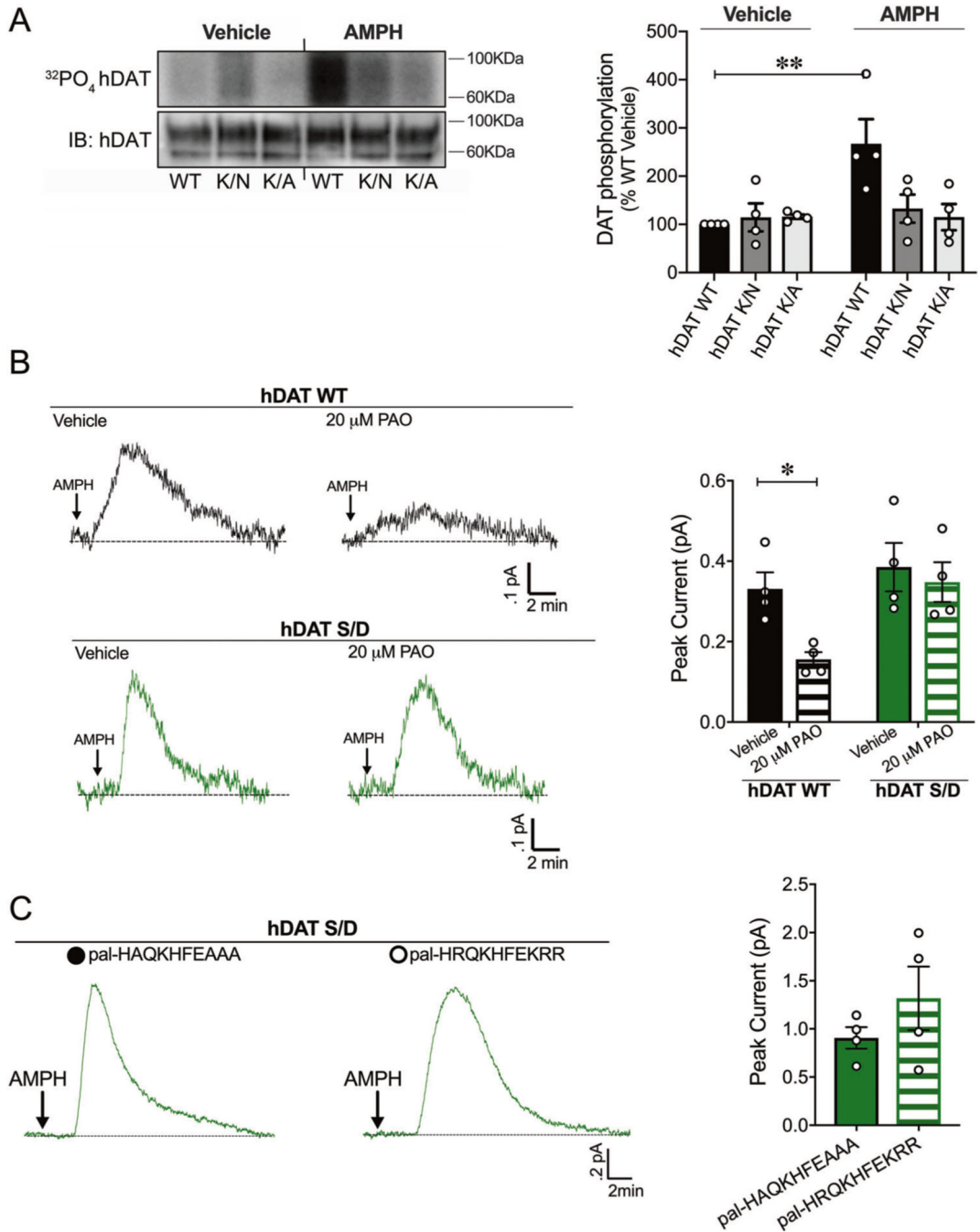


**Fig. 1. PIP<sub>2</sub>/N-terminus interactions regulate DAT phosphorylation, a posttranslational modification that supports PIP<sub>2</sub> independent DA efflux.**

**a** hDAT WT, hDAT K/N, or hDAT K/A cells were labeled with <sup>32</sup>P prior to vehicle or AMPH (10 μM, 30 min) incubation. Equal amounts of DAT determined by immunoblotting were immunoprecipitated and subjected to SDS-PAGE/auto-radiography. Left: representative autoradiographs showing hDAT phosphorylation after vehicle or AMPH exposure, along with respective immunoblots of total hDAT. Right: DAT phosphorylation is quantified as <sup>32</sup>P labeling normalized to basal hDAT <sup>32</sup>P labeling. hDAT WT

phosphorylation increased post-AMPH treatment relative to vehicle ( $n = 4$ ;  $F_{(2, 18)} = 5.05$ ,  $p = 0.002$ ). In hDAT K/N and hDAT K/A cells, displayed no changes in DAT phosphorylation in response to AMPH compared with vehicle ( $p > .05$ ). **b** Left: representative traces of amperometric currents recorded from hDAT WT (black traces) and hDAT S/D (green traces) preincubated in either vehicle or PAO (20  $\mu$ M, 10 min) and subsequently treated with AMPH (10  $\mu$ M; indicated by arrow). Right: quantitation of mean peak current amplitudes in hDAT WT and hDAT S/D cells. Preincubation with PAO significantly decreased DA efflux in hDAT WT cells ( $0.33 \pm 0.04$  pA) with respect to vehicle ( $0.16 \pm 0.02$  pA;  $p = 0.03$ ;  $n = 4$ ), but not in hDAT S/D cells (vehicle:  $0.38 \pm 0.06$  pA, PAO:  $0.35 \pm 0.05$  pA;  $p > 0.05$ ;  $n = 4$ ). **c** Representative traces from hDAT S/D cells after whole-cell patch delivery of control peptide (3  $\mu$ M, pal-HAQKHFEAAA) or PIP<sub>2</sub> sequestering peptide (3  $\mu$ M, pal-HRQKHFEKRR) to the cytoplasm of the cell prior (10 min) to the application of AMPH (10  $\mu$ M, indicated by arrow). Delivery of control or PIP<sub>2</sub> sequestering peptides resulted in comparable peak currents in response to AMPH ( $n = 4$ ;  $p > 0.05$ ). Data are presented as mean  $\pm$  SEM. Two-way ANOVA with Bonferroni's multiple comparison test: **a, b**; Student's *t* test: **c**.

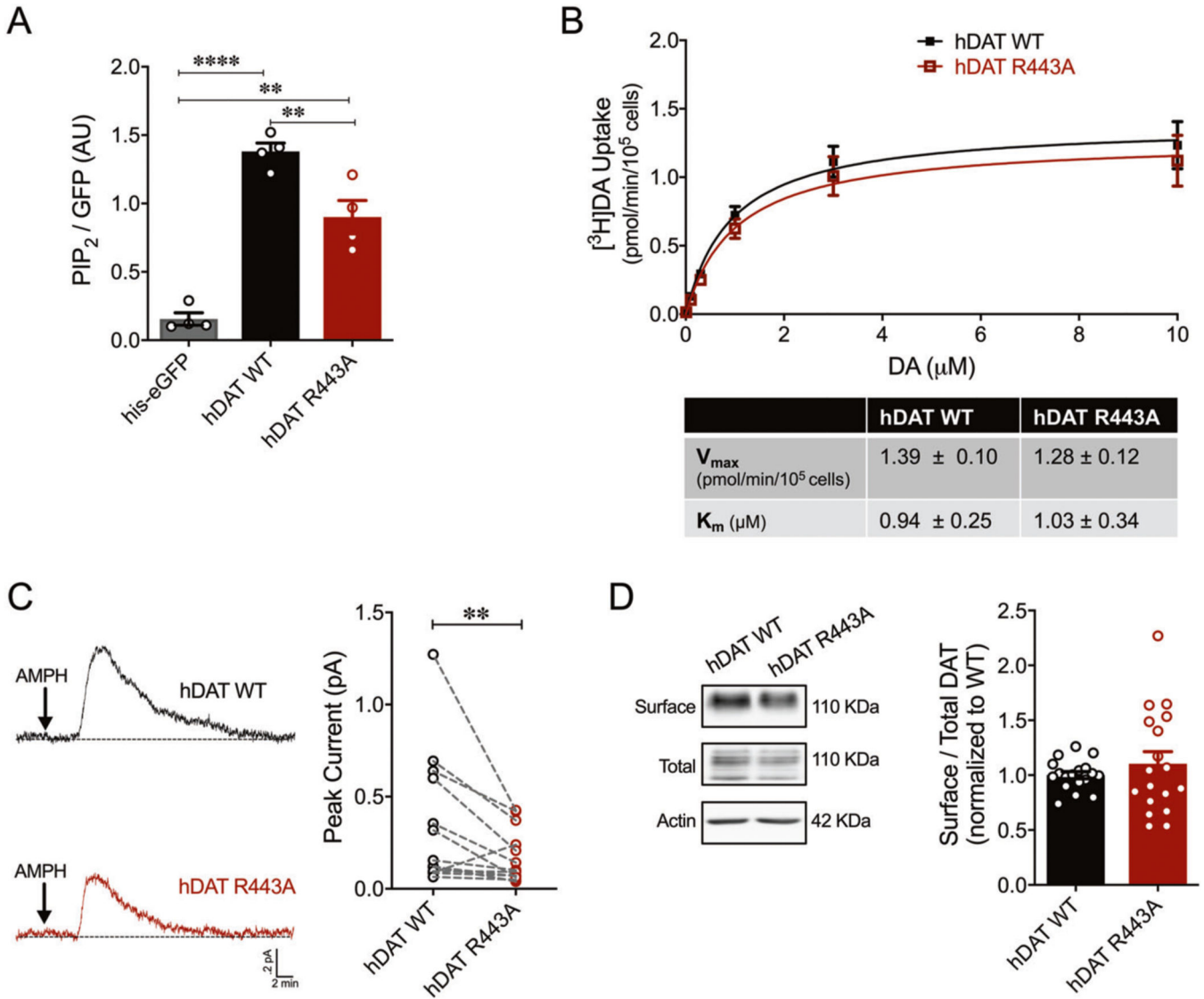


**Fig. 2. R443A substitution reduced PIP<sub>2</sub> binding and inhibited AMPH-induced DA efflux in vitro.**

**a** hDAT WT or hDAT R443A (containing a His-eGFP tag on the N-terminus) were purified from cellular extracts. Solubilized hDAT WT or hDAT R443A proteins were incubated with a water-soluble analog of PIP<sub>2</sub> conjugated to an orange fluorophore (BODIPY<sup>®</sup> TMR-PIP<sub>2</sub>). Specific binding was quantified as a ratio of PIP<sub>2</sub> fluorescence to eGFP. Minimal PIP<sub>2</sub> binding was measured in the presence of His-eGFP only (0.16 ± 0.05 AU) relative to hDAT WT (1.38 ± 0.12 AU) or hDAT R443A (0.90 ± 0.24 AU) ( $F_{(2,9)} = 55.11$ ,  $p < 0.0001$ ;  $n = 4$ ). hDAT R443A displayed a 34.8 ± 9.9% reduction in PIP<sub>2</sub> binding compared with hDAT WT ( $p = 0.007$ ). **b** Top: average [<sup>3</sup>H]DA saturation curves of DA uptake measured in hDAT WT (closed squares) or hDAT R443A (open squares) cells ( $n = 4$ , in triplicate). Curves were fit to Michaelis–Menten kinetics to derive  $K_m$  and  $V_{max}$ . DA uptake for hDAT R443A was comparable to hDAT WT at every DA concentration measured ( $F_{(1,120)} = 1.40$ ,  $p > 0.05$ ), as were the kinetic constants,  $K_m$  and  $V_{max}$  ( $p > 0.05$ ). **c** Left: representative traces of amperometric currents (DA efflux) recorded from hDAT WT (top) and hDAT

R443A (bottom) cells, in response to AMPH application (10  $\mu$ M, indicated by arrow). Right: quantitation of peak current amplitudes. hDAT R443A display a  $50.6 \pm 15.1\%$  decrease in AMPH-induced DA efflux relative to hDAT WT ( $p = 0.003$ ;  $n = 14$ ). **d** Left: representative immunoblots of surface hDAT (top), total (glycosylated and nonglycosylated) hDAT (middle), and actin as loading control (bottom). Right: hDAT expression is quantified as a ratio of surface to total glycosylated hDAT normalized to hDAT WT. hDAT R443A and hDAT WT had comparable expression ( $p > 0.05$ ;  $n = 6$ , in triplicate). Data are presented as mean  $\pm$  SEM. One-way ANOVA with Bonferroni's multiple comparisons test: **a**; two-way RM ANOVA with Bonferroni's multiple comparison test: **b**; Student's  $t$  test: **b**, **d**; Wilcoxon matched-pairs signed rank test: **c**.

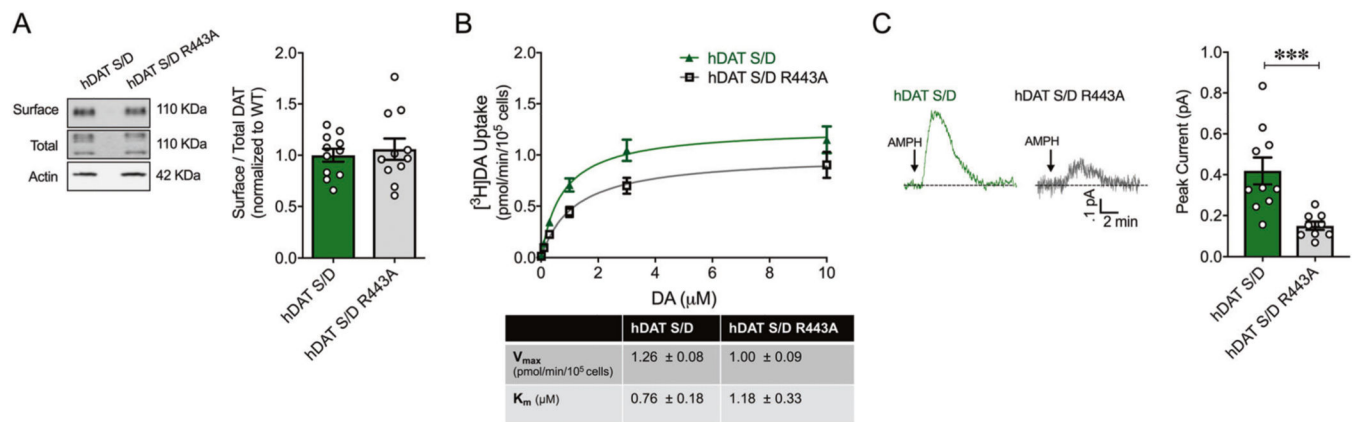


**Fig. 3. Disrupting R443 electrostatic interactions inhibits DA efflux independent of DAT N-terminus phosphorylation.**

**a** Left: representative immunoblots of surface hDAT (top), total hDAT (middle), and actin (bottom). Right: hDAT expression is quantified as a ratio of surface to total glycosylated hDAT normalized to hDAT S/D. hDAT S/D R443A had comparable expression to hDAT S/D ( $p > 0.05$ ;  $n = 4$  in triplicate). Dashed lines indicate separate sets of experiments. **b** Top: average <sup>3</sup>[H]DA uptake kinetics measured in hDAT S/D R443A (gray line open squares) and hDAT S/D (green line closed triangle) cells ( $n = 4$ , in triplicate). Curves were fit to Michaelis–Menten equation to derive  $K_m$  and  $V_{max}$ . Bottom: the  $V_{max}$  and  $K_m$  for hDAT S/D R443A were comparable to hDAT S/D cells ( $p > 0.05$ ). **c** Left: representative traces of DA efflux recorded from hDAT S/D (green trace) and hDAT S/D R443A cells (gray trace) in response to AMPH application (10 μM, indicated by arrow). Right: quantitation of peak current amplitudes ( $n = 9–10$ ). DA efflux from hDAT S/D R443A ( $0.15 ± 0.02$  pA;  $p = 0.01$ ) was significantly lower compared with hDAT S/D cells ( $0.42 ± 0.07$  pA;  $p = 0.0004$ ). Data are presented as mean ± SEM. Student's *t* test: **a–c**; two-way RM ANOVA with Bonferroni's multiple comparison test: **b**.

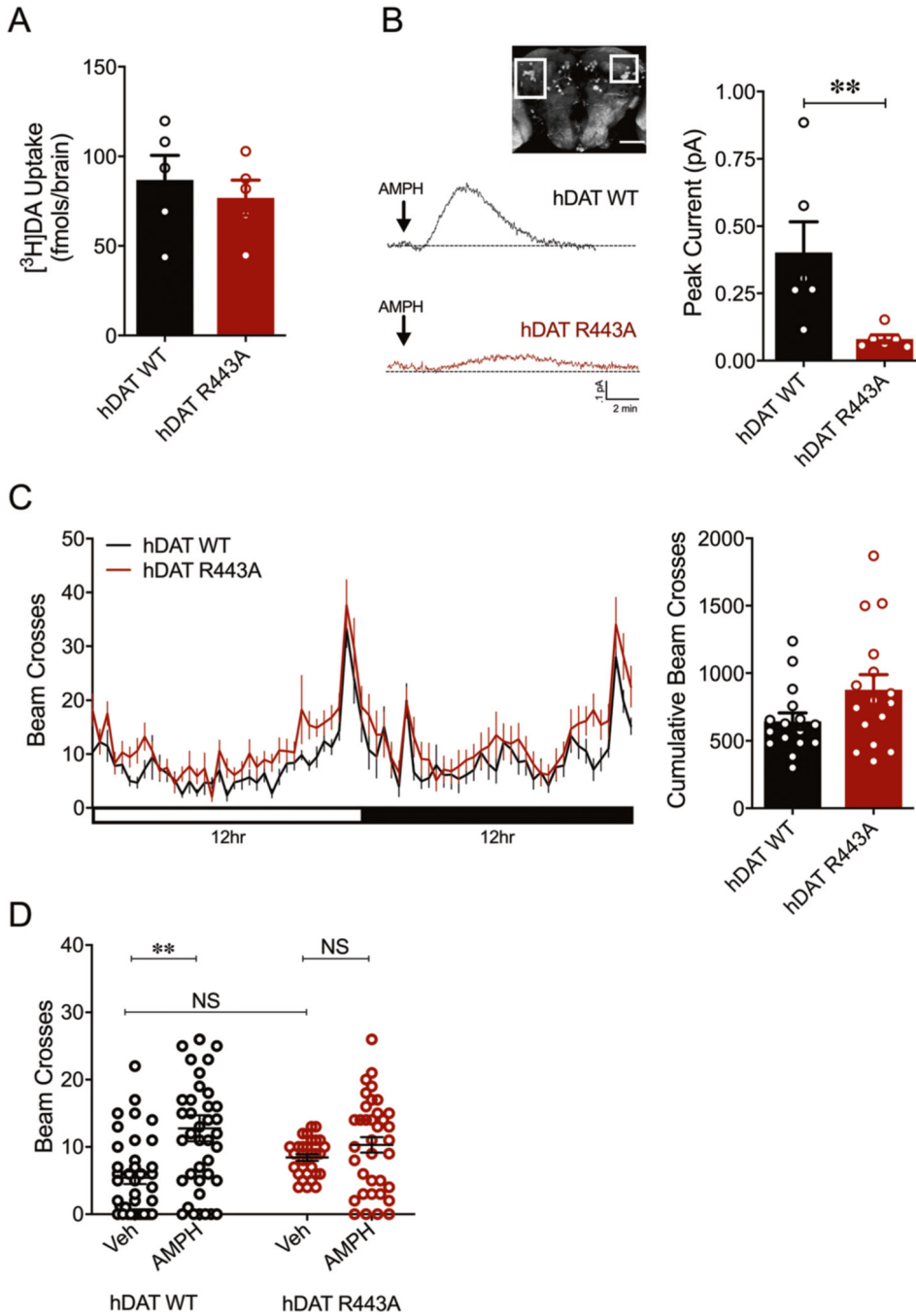


**Fig. 4. hDAT R443A limits central and behavioral responses to AMPH.** **a** hDAT WT or hDAT R443A was expressed in DA neurons in a dDAT KO (*fmn*) background. [<sup>3</sup>H]DA uptake (200 nM, 10 min) was measured in adult isolated *Drosophila* brain (*n* = 5). DA uptake measured in hDAT WT flies (86.9 ± 13.7 fmol/brain) was comparable to that measured in hDAT R443A flies (76.9 ± 9.9 fmol/brain; *p* > 0.05). **b** Left: representative traces of amperometric currents recorded from a dense cluster of DA neurons (PPL1, boxed in inset) in response to AMPH application (20 μM; indicated by arrow) in hDAT WT (black trace) and hDAT R443A (red trace) brains. Right: quantitation

of peak current amplitudes. hDAT WT flies displayed higher peak currents ( $0.40 \pm 0.11$  pA) than hDAT R443A flies ( $0.08 \pm 0.02$  pA;  $n = 6$ ;  $p = 0.004$ ). **c** Left: locomotor activity was assayed over a 24-h period including both the light (horizontal white bar) and dark (horizontal black bar) cycle. Circadian activity curves show average beam crosses (20-min interval) during the 24-h period for hDAT WT (black line) and hDAT R443A (red line) *Drosophila*. Right: cumulative beam crosses were not significantly different for hDAT WT ( $654 \pm 61$ ) versus hDAT R443A *Drosophila* ( $879 \pm 110$ ;  $p > 0.05$ ;  $n = 16$ ). **d** Locomotor activity was measured after a 30-min exposure to vehicle or 1 mM AMPH. The total beam crosses increase in the AMPH ( $12.8 \pm 1.9$ ;  $n = 39$ ) compared with vehicle group ( $5.4 \pm 0.9$ ;  $n = 38$ ) of hDAT WT *Drosophila* ( $F_{(1,138)} = 11.83$ ,  $p = 0.0005$ ). In hDAT R443A *Drosophila*, AMPH ( $10.3 \pm 1.2$ ;  $n = 36$ ;  $p > 0.05$ ) did not increase the total beam crosses compared with vehicle group ( $8.5 \pm 0.5$ ;  $n = 29$ ) and with respect to hDAT WT vehicle group ( $p > 0.05$ ). Data are presented as mean  $\pm$  SEM. Student's *t* test: **a**, **c**; Mann–Whitney test: **b**; two-way ANOVA with Bonferroni's multiple comparison test: **d**.



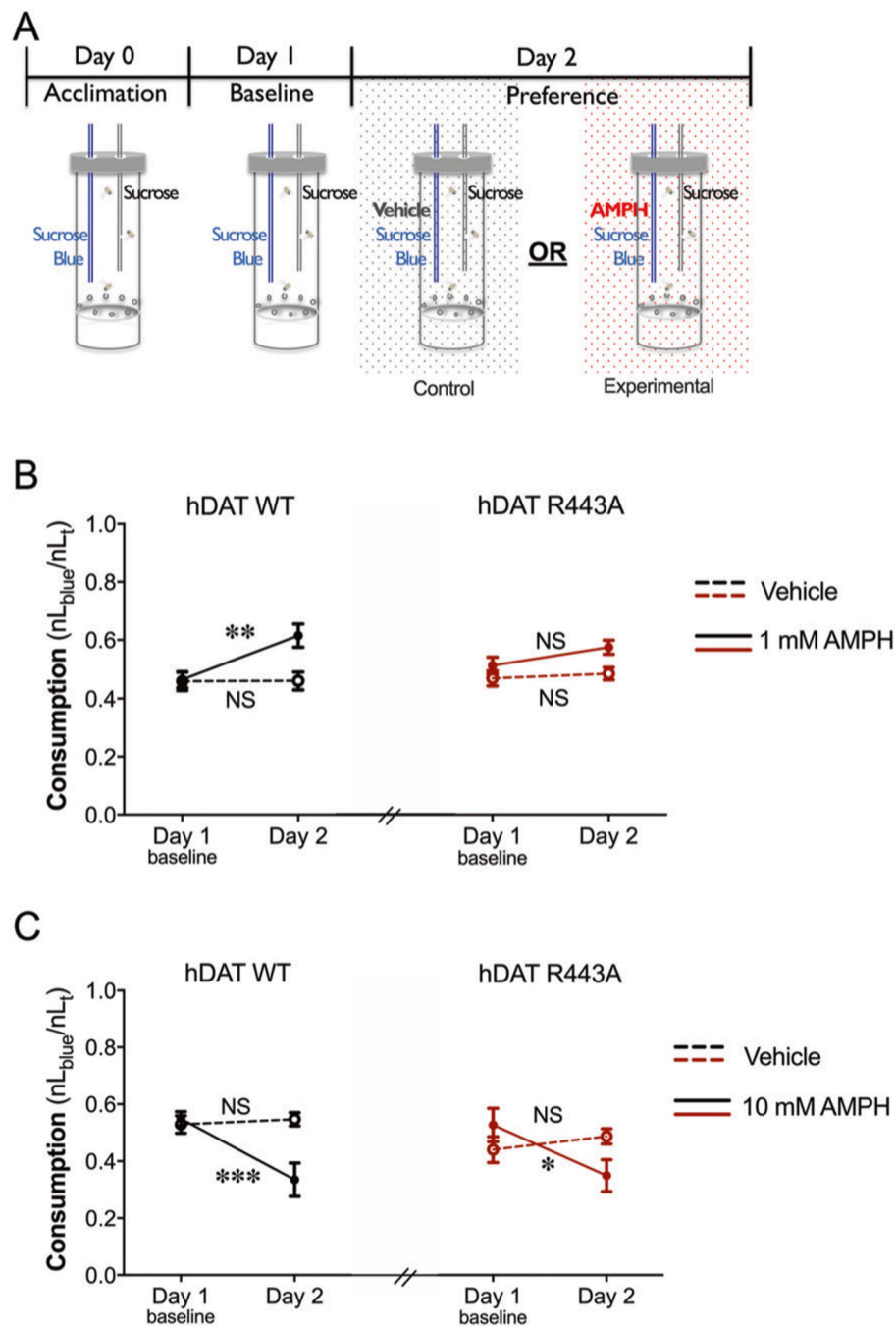


**Fig. 5. In a two-choice consumption paradigm, hDAT R443A flies display diminished AMPH preference and continued AMPH aversion.**

**a** Schematic illustrating a two-choice consumption paradigm developed to measure AMPH preference in flies. The paradigm is comprised of three 24-h testing periods: acclimation, baseline, and preference, where capillaries were replaced every 24-h period to measure AMPH consumption. Adult *Drosophila* were placed in custom chambers containing two volumetric capillaries filled with either clear (100 mM sucrose) or blue food (100 mM sucrose, 500  $\mu$ M blue). During AMPH preference testing, blue food was supplemented with either AMPH (1 mM or 10 mM) for experimental groups (solid line) or vehicle for

control groups (dashed line). Preference is presented as a ratio of blue food to total food consumption. **b** Left: hDAT WT *Drosophila* exposed to 1 mM AMPH (solid black line) consumed more AMPH ( $61.5 \pm 4.0\%$ ) relative to baseline vehicle ( $46.3 \pm 2.8\%$ ;  $n = 12-13$ ,  $F_{(1, 49)} = 5.23$ ,  $p = 0.005$ ). hDAT WT control groups consumed equal amounts of blue food during day 1 ( $45.8 \pm 3.1\%$ ) and day 2 ( $46.0 \pm 3.0\%$ ;  $n = 14$ ;  $p > 0.05$ ). Right: hDAT R443A *Drosophila* (solid red line) did not consume more AMPH ( $57.4 \pm 2.4\%$ ) compared with baseline vehicle ( $51.1 \pm 2.8\%$ ;  $n = 13$ ,  $F_{(1, 50)} = 0.86$ ,  $p > 0.05$ ). hDAT R443A control groups consumed comparable amounts of blue food during day 1 ( $46.7 \pm 2.6\%$ ) and day 2 ( $48.3 \pm 2.2\%$ ;  $n = 14$ ,  $p > 0.05$ ). **c** Left: hDAT WT *Drosophila* exposed to 10 mM AMPH (solid black line) consumed drastically less AMPH ( $33.5 \pm 5.9\%$ ) compared with baseline vehicle ( $54.9 \pm 2.5\%$ ;  $n = 12$ ;  $F_{(1, 44)} = 9.55$ ,  $p = 0.0004$ ). Control groups for hDAT WT (black dashed line) consumed comparable food on day 1 and day 2 ( $n = 12$ ;  $p > 0.05$ ). Right: hDAT R443A *Drosophila* consumed significantly less 10 mM AMPH ( $35.0 \pm 5.6\%$ ) compared with baseline vehicle ( $52.9 \pm 5.9\%$ ;  $n = 11$ ;  $F_{(1, 39)} = 5.18$ ,  $p = 0.03$ ). Control groups for hDAT R443A (red dashed line) consumed comparable food on day 1 and day 2 ( $n = 10-11$ ;  $p > 0.05$ ). Each data point represents the mean of 10–14 measurements  $\pm$  SEM. Two-way ANOVA with Bonferroni's multiple comparison test: **b, c**.